PERGAMON

Aerosol Science 34 (2003) 765–782

Journal of
Aerosol Science

www.elsevier.com/locate/jaerosci

Microparticle detachment from surfaces exposed to turbulent air flow: controlled experiments and modeling

A.H. Ibrahim, P.F. Dunn*, R.M. Brach

Particle Dynamics Laboratory, Department of Aerospace and Mechanical Engineering, University of Notre Dame, 107 Hessert Center, Notre Dame, IN 46556, USA

Received 30 October 2002; received in revised form 2 February 2003; accepted 4 February 2003

Abstract

This work presents the results of experiments conducted to characterize the detachment of microparticles from surfaces exposed to turbulent air during accelerated free-stream flow. Smooth glass plates used as substrates are scanned with an atomic force microscope to determine their roughness-height distributions. Microparticles of different sizes, materials and shapes (mostly microspheres) are deposited as sparse monolayers onto the substrates under controlled clean and dry conditions. The microparticles attach to the substrate in a condition of static equilibrium due to adhesion and reside completely within the viscous sublayer as the flow is accelerated. Microvideographic observations of individual microparticle detachment show that detachment occurs primarily as rolling motion along the surface and not as lift-off. Detachment is not necessarily followed by entrainment in the flow. Results are presented as detachment fractions as function of time.

The experimental results reveal that detachment is governed by a balance of the moments of aerodynamic drag and rough-surface pull-off forces. This is substantiated using a recently developed attachment theory that takes into account surface roughness to determine the pull-off force of microparticles. The sensitivity of the free-stream threshold velocity for detachment to five factors contained in the experiments and the model is analyzed. Results indicate that the surface energy of adhesion and the microsphere radius have the most influence on the threshold velocity for detachment.

Keywords: Adhesion to surfaces; Detachment from surfaces; Particle adhesion; Surface forces

1. Introduction

Microparticle detachment from a surface and subsequent entrainment into air flow occurs under many conditions. For example, microparticles acting as carriers of smoke particulates can be

* Corresponding author.
E-mail address: pdunn@nd.edu (P.F. Dunn).

0021-8502/03/$ - see front matter
doi:10.1016/S0021-8502(03)00031-4

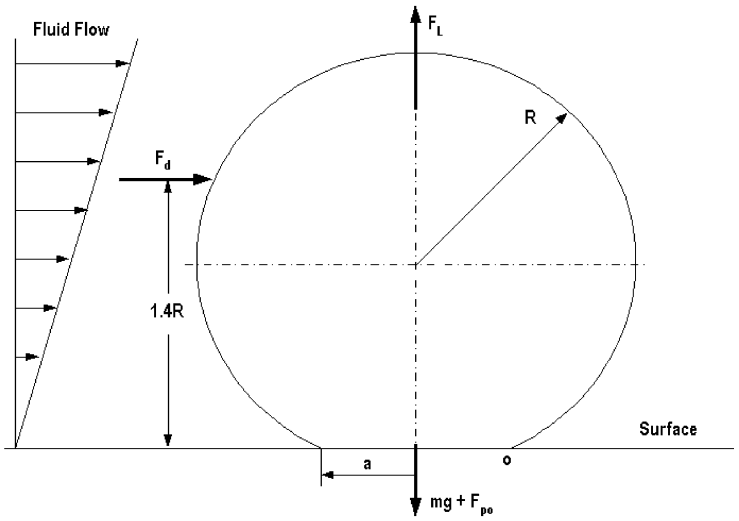

Fig. 1. Microparticle on a surface in a linear, mean shear flow.

resuspended into room air from ventilation systems. Other common instances occur in filtration, saltation and air pollution. Extensive reviews have been made of adhesion forces by Bowling (1988) and Ranade (1987), and of the resuspension of microparticles from surfaces by Ziskind, Fichman, and Gutfinger (1995), Nicholson (1988) and Sehmel (1980). However, few experiments have investigated systematically the effects of microparticle size, shape, material and humidity and few investigators have reported directly observed modes of resuspension or the repeatability of their results.

In this paper, detachment refers to the process of separation by rolling, sliding or direct lift-off of a microparticle adhering in static equilibrium to a surface. Entrainment is the capture of the microparticle by the flow after being detached. Re-entrainment (or resuspension) is the removal of a microparticle from a surface, where the microparticle previously was airborne and subsequently was deposited on the surface.

A microparticle can be considered to be in a state of static equilibrium when it is attached to a fixed surface (substrate) by adhesion. Its environment includes a substrate and a fluid flow that exerts aerodynamic forces and moments on the microparticle. Fig. 1 shows a microsphere of radius R adherent to a surface through a circular contact area of radius a. The microsphere is held on the surface by its gravitational (mg) and adhesion forces (F_{po}). If the microsphere is contained within the viscous sublayer, it experiences a linear mean shear flow that produces drag and lift forces (F_{d} and F_{L}) as well as moments of these forces. The present work investigates the conditions under which a fluid flow will cause a microparticle to detach under these conditions from the surface.

Detachment situations usually are characterized in terms of either a free-stream velocity, U, or a friction velocity, u^*. The friction velocity is defined as $\sqrt{\tau_{\mathrm{w}}/\rho}$, where τ_{w} is the wall shear stress and ρ is the density of the flowing medium. In the present work, the friction velocity is related to the free-stream velocity using an expression developed from a subsidiary calibration experiment. The detachment rate, Λ, is the ratio of the average detachment flux (number of particles detached/m^2/s)

to the initial number of particles per unit surface area (number of particles/m^2). A useful and common measure follows from the detachment rate, which is the fraction of detachment, F, where $F = \sum_i \Lambda_i \Delta_{ti}$, in which Δ_{ti} is the duration of the ith sample period.

Wind tunnel experiments typically involves two phases. During the first phase, the flow is accelerated for a period of time and some microparticles are removed either in groups or individually. The second phase corresponds to when the mean flow reaches a steady state. As is found from the present study, the detachment rate is coupled to the flow acceleration. The detachment rates during the first phase can be as much as two orders of magnitudes more than the rates during the second phase. The primary emphasis in the current work is on the detachment during the first phase, i.e., during flow acceleration.

Few experimental studies have observed and reported the actual mode of detachment. Masironi and Fish (1964) observed combinations of lift-off and motion along the surface (i.e., rolling and/or sliding). Similarly, few experimental studies mention the repeatability of their detachment/resuspension data. Wu, Cliff, and Russell (1992) and Braaten, Paw, and Shaw (1990) found large changes in resuspension fractions for runs repeated under the *same* conditions. Smedley, Phares, and Flagan (1999) achieved small variability in their microparticle removal experiments by careful surface preparation.

The resuspension rate is reduced at high relative humidity. This is because of the adsorption of water vapor at the particle-surface interface and its effects on adhesion. Corn (1961) and Corn and Stein (1965) found almost no change in adhesion forces with relative humidities up to 30% and a rapid increase thereafter. Despite the large dependence of the resuspension on relative humidity, many experiments do not report the value of the relative humidity. Many runs are made on different days at different relative humidities, which further adds to uncertainty in the results.

Surface-roughness effects on resuspension also must be considered because actual surfaces are rough. Roughness of the order of the atomic scale always is present, even for nominally "smooth" surfaces. Kim, Rockfold, and Russell (1999) reveal that a surface roughness of only 45 Å is sufficient to reduce the pull-off force to a very small fraction of its value for smooth surface. Soltani (1993) shows for hard elastic materials that a surface roughness of the order of the atomic scale can reduce adhesion significantly. According to the results of Cheng, Brach, and Dunn (2002), a standard deviation of heights of 17 Å can cause the pull-off force to be reduced to 1% of its smooth-surface value.

Particle–particle collisions have a significant effect on resuspension. Once a few microparticles are detached, they move along the surface and impact other microparticles. This process supplies enough momentum to the stationary microparticles to overcome their adhesion with the substrate; they detach and may resuspend into the flow. Fairchild and Tillery (1982) found that the saltation of 200 μm diameter particles increases the maximum vertical particle flux by two orders of magnitude. The present work deals with sparse monolayers of microparticles, where particle–particle collisions play a relatively minor role.

Many models use the concept of turbulent bursts to explain detachment and entrainment. A number of investigators (e.g., Kline, Reynolds, Schraub, and Runstadler (1967) and Robinson (1991)) have studied the turbulent-burst phenomenon. Yung, Merry, and Bott (1989) used flow visualization in the turbulent flow of *water* to examine the interaction between turbulent burst-sweep events and microparticles *completely embedded within the viscous sublayer*. These results suggested that, in general, turbulent burst-sweep events are insignificant in the re-entrainment process, although some of the microparticles were re-entrained by such events.

The present work investigates the detachment of stainless steel and glass microspheres, and Lycopodium spore microparticles from a glass substrate. Frames from microvideographic recordings of individual microparticle motion were examined. This permitted a quantitative evaluation of the progress of detachment in relation to flow velocity. The overall approach was to conduct well-defined and controlled experiments such that a comparison between experiment and model could be made without adjusting any coefficient values a posteriori to obtain better agreement.

The major factors controlled in the experiments included the air-flow acceleration, the final free-stream velocity, relative humidity, initial number density of deposited microparticles, microparticle counting technique and microparticle material and size. The substrate surface was scanned with an atomic force microscope (AFM). The resulting distribution of surface heights was used directly in the model of Cheng et al. (2002) to predict the microparticle pull-off force. This information was coupled with a model of the forces and moments acting on the microparticle. This subsequently provided estimates of the flow velocity needed to detach the microparticles, which could be compared directly with the experimental results.

In the following, the experimental facility, procedures and conditions are described first. Then the experimental results are presented, including first some qualitative observations of detachment and then more detailed findings. These results are compared with a model of the detachment process. Finally, the parameters that significantly influence microparticle detachment are identified through a sensitivity analysis based upon the model presented.

2. Description of experiments

A schematic of the experimental facility is shown in Fig. 2. Air is drawn through a contraction section containing 12 screens (1.05 m long; contraction ratio 27:1), an inlet section (1 m long;

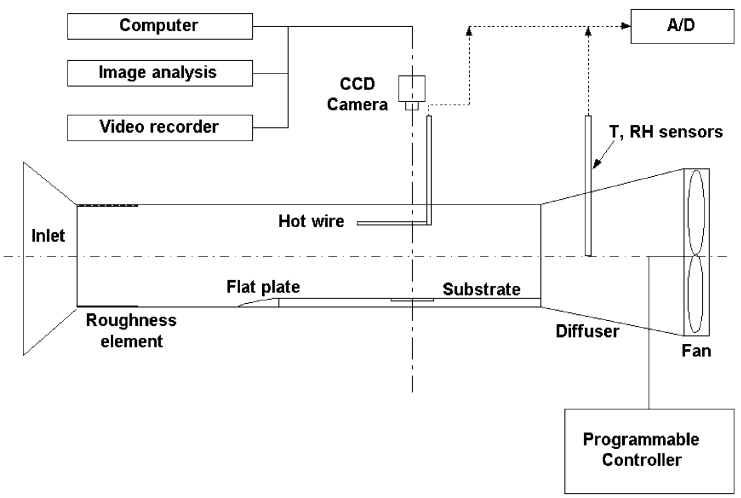

Fig. 2. Schematic of the wind tunnel used to study microparticle detachment.

distributed roughness element at its beginning to produce boundary layer turbulence), a test section (1 m long; 20.3 cm × 20.3 cm) and a diffuser section (1.05 m long; four-blade fan and 7.5 HP motor). The wind tunnel is equipped with a programmable controller to set the steady-state velocity and the acceleration during the transient phase. The diffuser is equipped with a type-K thermocouple and a relative humidity sensor. Both are connected to a voltage amplifier and data-acquisition board (National Instruments 6023 E).

The test section includes a smooth flat plate at its bottom that is 1.05 m long with a leading wedge angle of 10°. The flat plate contains a grove designed to accommodate a glass substrate (Amersham Pharmacia; 10 cm width × 10.5 cm length × 1.27 mm thickness).

The free-stream velocity can be varied from zero up to ~23 m/s. The flow velocity is accelerated from zero up to the prescribed steady-state velocity almost linearly with time. The transient velocity profile can be fitted with a linear fit at an r^2 value of 99.4%. Flow cross-sectional and length-wise developments have been assessed using single hot-wire anemometry and are controllable to within 5%. Transient profiles are repeatable to within 3%. Free stream turbulence intensity is less than 1% over the entire velocity range. The motion of the microparticles is recorded using a 30 frames/s CCD camera (Astrovid 2000). Optical lenses (Olympus) are attached to the camera to achieve enough magnification (typically about 20×) to resolve individual microparticle motion. The camera output is connected to a digitizer and a frame grabber in a personal computer for image analysis. The field of view is 13.7 mm × 10.2 mm for most cases.

Microvideographic images and free-stream velocity measurements are obtained simultaneously. The image acquisition is synchronized with the velocity measurement by a flash. Consequently, the number of microparticles on the surface is known at any time as a function of free-stream or friction velocity.

Microparticles (Duke Scientific) were selected to satisfy the following conditions: commercially available, relatively mono-disperse in size, can be deposited on the surface as singlets, spherical or nearly spherical in shape, detach in the velocity range available in the wind tunnel and can be contained completely within the viscous sublayer. The microspheres used were stainless steel (diameter: 64–76 μm; density: 8000 kg/m^3; Poisson's ratio: 0.28; Young's modulus: 215 GPa; hereafter referred to as SS70), glass (soda lime glass; diameter: 68.2–77 μm; density: 2420 kg/m^3; Poisson's ratio: 0.27; Young's modulus: 80.1 GPa; hereafter referred to as GL72), and similar glass microspheres (diameter: 29.7–34.1 μm; hereafter referred to as GL32). Lycopodium spores (diameter: 25–35 μm; hereafter referred to as LY30) were used to study non-spherical microparticles of similar diameter. More polydisperse stainless steel microspheres (diameter: 10–65 μm; hereafter referred to as SSPOLY) were used as an example of poly-disperse microspheres.

All experiments were conducted at a temperature of ~23°C and a relative humidity of 25 ± 3%. The microparticles were deposited as a monolayer on the glass substrate to avoid any cohesive forces between the microparticles. Deposition was made immediately before initiation of flow. The number of deposited microparticles was such that it was large enough to achieve acceptable statistical accuracy but not too large to cause an unacceptable number of collisions on the surface. This amounted to depositing, on the average, approximately 60 microparticles over the field of view, resulting in a number density of microparticles on the order of magnitude of 1 microparticle/mm^2. Any agglomerates or microparticles removed by collisions were excluded from the count, which typically was about 7% of the microparticles. Experimental repeatability was assessed by repeating the experiment under the same conditions.

Table 1
Distribution of the standard deviations of the heights on the glass substrate as measured by AFM

Standard deviations of heights (Å)	Number of occurrences
10.8	7205
24.9	1676
39.0	821
53.0	224
67.1	41
81.2	14
95.3	1
109.4	1
123.4	5
137.5	12

Similar glass substrates were used for all cases. The substrate was prepared prior to each experiment by cleaning it with phosphate-free detergent, immersing it in dilute nitric acid (1:1) for 60 s, rinsing it in distilled water for 120 s and then heating it at 200°C for 1 h. All substrates were kept in a dry, warm enclosure until used. This surface preparation technique was similar to that given by Phares, Smedley, and Flagan (2000).

One of the glass substrates was scanned by AFM. The scan area was 100 μm × 100 μm. The distribution of the surface height standard deviations is shown in Table 1. Values of the standard deviation were obtained from 10,000 samples of reduced area (20 μm × 20 μm) that were selected randomly from the total scan area. The mean of the standard deviations was 17 Å. The ratio of the rough-to-smooth surface pull-off forces (hereafter referred to as C) as determined from the theory of Cheng et al. (2002) was ~0.01. A sample of the stainless steel microspheres was examined using a scanning electron microscope. Their surface appeared "smooth" to within the resolution of the instrument (Caylor, 1993).

The friction velocity, u^*, was calibrated against the free-stream velocity, U, in two independent ways using a Preston tube (Bechert, 1996) and oil-film interferometry (Zilliac, 1996). The Preston tube technique assumes a fully developed turbulent flow that satisfies the logarithmic law of the wall. The oil-film technique does not assume logarithmic law-of-the-wall behavior. The results of the two measurements compared well with each other and with the empirical relation of Schlichting (1979) that assumes fully developed turbulent flow satisfying the logarithmic law of the wall. This comparison is shown in Fig. 3. Agreement among the three methods verifies that the flow in the test section is fully developed turbulent flow. The velocities (in units of m/s) are correlated through a least-squares linear regression by the equation

$$u^* = 0.0375U + 0.0387, \tag{1}$$

where the uncertainty in the friction velocity is ±0.0300 at a 95% confidence level.

The experimental cases were chosen to illustrate the effect of specific variables on detachment. Comparisons between the results of the SS70 and GL72 cases show the effects of adhesion surface

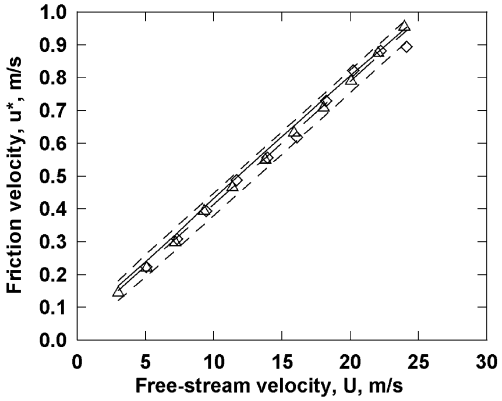

Fig. 3. Friction velocity calibrated with the free-stream velocity by oil-film interferometry (◇), and Preston tube (△). The dashed line is the best fit obtained for these measurements. The dotted lines are the 95% confidence limits. The solid line is the empirical relationship of Schlichting (1979).

energy and particle density for nominally the same diameter (the model predicts that particle density has a negligible effect in this diameter range). Comparisons between the results of the GL72 and GL32 cases reveal the effect of diameter for the same particle/surface combination. Comparisons between the results of the GL32 and LY30 cases display the combined effect of particle sphericity and adhesion energy for the same nominal diameter. For all comparisons, the flow was accelerated linearly from zero velocity to a prescribed velocity (typically 11 or 23 m/s) over a specific period of time (typically 60 or 150 s, respectively).

3. Experimental results

The mechanics of detachment can be observed using microvideography. The qualitative aspects of detachment are shown in Fig. 4. This figure displays some selected frames of an experiment using the SS70 microspheres. The video frame rate was 1/30 s and each frame area was 3.95 mm × 2.84 mm. The first frame (frame #0) was taken when the free-stream velocity was ∼1.6 m/s and the last frame (frame #19) when it was ∼1.7 m/s. The pictures in the figure were obtained using dark-field imaging.

The behavior shown in Fig. 4 was characteristic of all the cases reported in this paper. Microparticle detachment on the surface occurred in discrete, intermittent events, either in groups or individually. When two or more microparticles detached simultaneously, some microparticles in between them did not detach. This is illustrated in the first 3 frames of the figure, in which two detached microparticles move to the left on the top of each frame without disturbing the ones in-between. Detachment and subsequent motion was observed to follow straight or curved paths, as shown in all of the frames. A collision causing detachment is shown on the right-hand side of frames #9, #10 and #14. Detachment rather than re-attachment occurred because of the moving microparticle's large momentum (its density is approximately 8000 times greater than that of air).

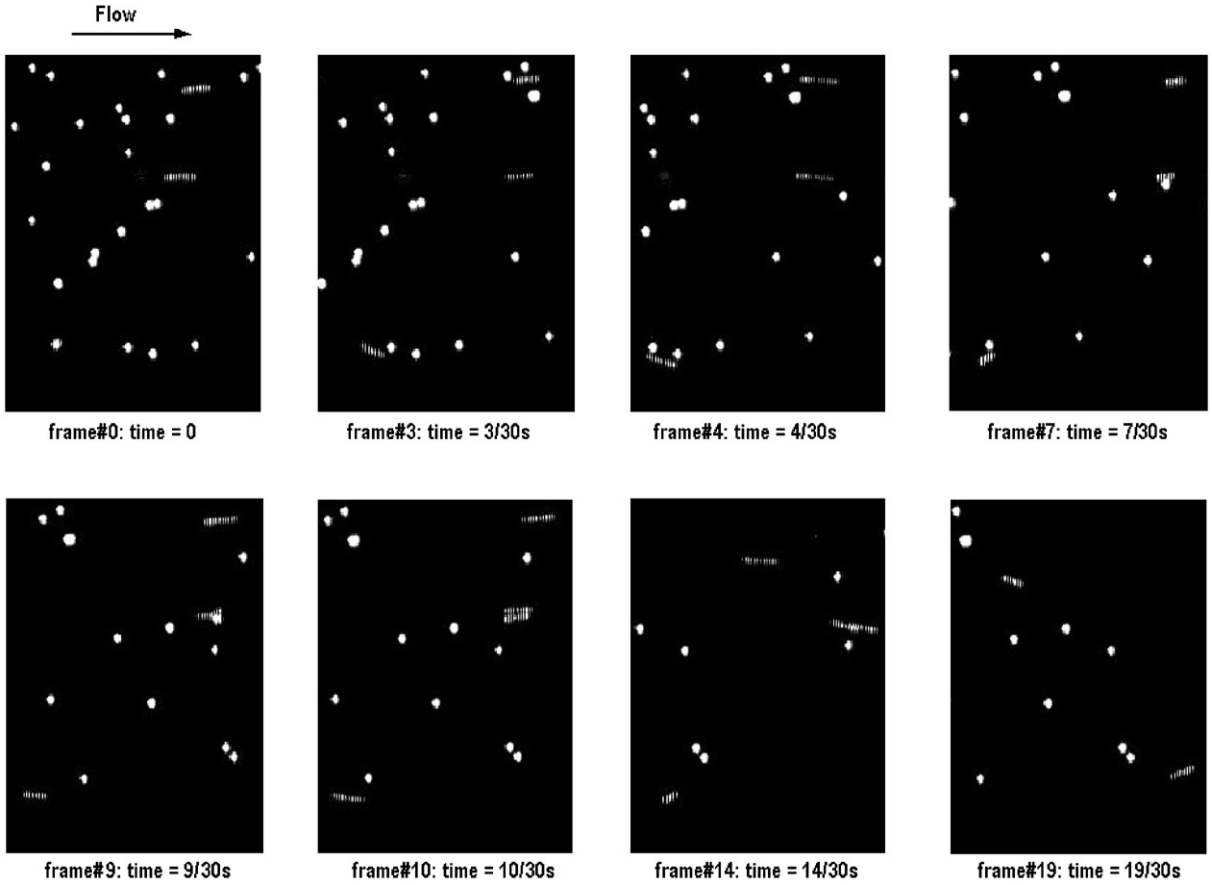

Fig. 4. Parts of some selected frames for SS70. Each frame area was 3.95 mm × 2.84 mm. The first frame was taken when the free-stream velocity was ∼1.6 m/s and the last frame when it was ∼1.7 m/s.

For the conditions of these experiments, microparticle detachment occurred as rolling and/or sliding rather than as direct lift-off. Fig. 4 illustrates typical detachment behavior as marked by the existence of the trace of the microparticles as they move along the surface. Modeling supports that this motion is rolling rather than sliding. Detachment was not necessarily followed by entrainment. Microparticles that remained adherent to the surface did not detach when subjected again to the same flow velocity history in a subsequent experiment. Further, all the microparticles did not detach at a single value of the free-stream velocity, but rather over a range of velocities. This was a consequence of the inherent variability in surface energy of adhesion, microparticle diameter, local flow velocity, surface roughness and Hertzian stiffness in the present experiments.

The experimental results that follow are presented as detachment fraction versus time or free-stream velocity. This fraction is defined as

$$n^*(t) = 1 - \frac{n(t)}{n(0)}, \tag{2}$$

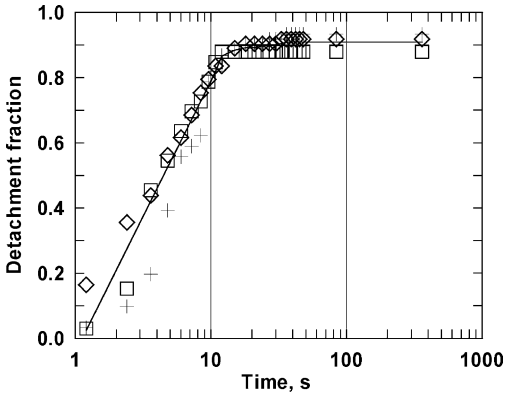

Fig. 5. Detachment fraction versus time for SS70 microspheres. The symbols show three repeated experiments. The free-stream velocity increased almost linearly with time up to 7 m/s in 11 s and then remained constant.

where $n(t)$ is the number of non-detached microparticles on the surface at time t. Ideally, for situations involving truly mono-disperse microparticles, molecularly smooth microparticles and substrate surfaces and perfectly controlled experimental conditions, all of the microparticles would detach at one velocity. However, because of variations in these variables and others, the microparticles will detach over a range of velocities. Thus, it is appropriate to define a threshold velocity for detachment, U_{th}, which is the velocity at which the detachment fraction equals 0.50. The uncertainty in U_{th} in the present work is ~10–20% at 95% confidence.

In the present experiments, two significantly different detachment rates (number of microparticles detached per second) were observed in every case. The first rate was approximately 600 times greater than the second. This difference in rates was associated directly with the acceleration of the flow. During flow acceleration, approximately 90% of the microparticles were detached. The remaining microparticles were detached over an extended period of time after the flow reached a constant, prescribed velocity.

Fig. 5 displays the temporal variation of the detachment fraction for SS70 microspheres on a glass substrate. The free-stream velocity was accelerated linearly with time up to 7 m/s in 11 s and then held constant. Two distinct phases of detachment were identified. The first phase is characterized by a high net detachment rate (4.6/s) and the second by a much lower net detachment rate (0.0075/s). The transition between the two phases occurred when the controlled free-stream velocity became constant. This can be explained by a balance between removing moments (drag and lift) and resisting moments (pull-off and gravity) acting on the microparticle. As long as the flow velocity increases in time, the removing moments increase while the resisting moments remain constant. Thus, more and more microparticles continually are removed. When the flow velocity becomes constant, only random events having drag and lift moments higher than the average can remove microparticles. This causes the detachment rate to decrease significantly. This observation suggests that the microparticles removed during the accelerated-flow phase have less adhesion moments than those removed during the steady-state phase. This is consistent with the observations of Phares et al. (2000).

Two sets of microspheres with the same nominal diameter but different material can be exposed to the same temporal variation in flow. Differences will occur in their detachment rates because of

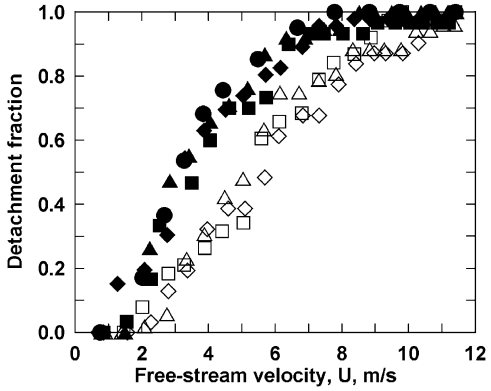

Fig. 6. Detachment fraction versus free-stream velocity: The solid symbols show four repeated experiments of SS70 and the open symbols show three repeated experiments of GL72. The free-stream velocity increased almost linearly with time up to ~11 m/s in 60 s in both experiments.

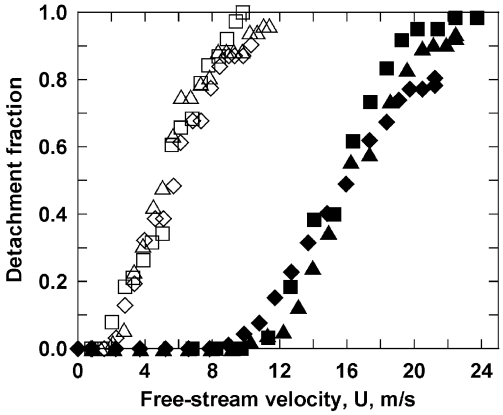

Fig. 7. Detachment fraction versus free-stream velocity: The solid symbols show three repeated experiments of GL32 microspheres and the open symbols show three repeated experiments of GL72 microspheres. The free-stream velocity increased almost linearly with time up to ~23 m/s in 150 s in the GL32 experiments.

differences in their densities and adhesion energies. Fig. 6 compares the detachment fraction versus free-stream velocity (hence time) of the SS70 and GL72 microspheres on a glass substrate. Each case was repeated several times to assess the repeatability of the results. The results reveal that almost all of the microspheres for both cases are detached by the time (60 s) that the flow velocity becomes constant (at ~11 m/s). The U_{th} for GL72 is higher than that for SS70 because glass microspheres on glass have a higher adhesion energy than stainless steel microspheres on glass (0.40 J/m^2 for GL72 versus 0.15 J/m^2 for SS70) and, therefore, a larger pull-off moment.

Fig. 7 compares the detachment fraction versus free-stream velocity of the GL72 and GL32 microspheres. The larger-diameter microspheres detach at lower free-stream velocities, between ~2 and ~10 m/s. The smaller-diameter ones detach between ~9 and ~23 m/s. This is because the

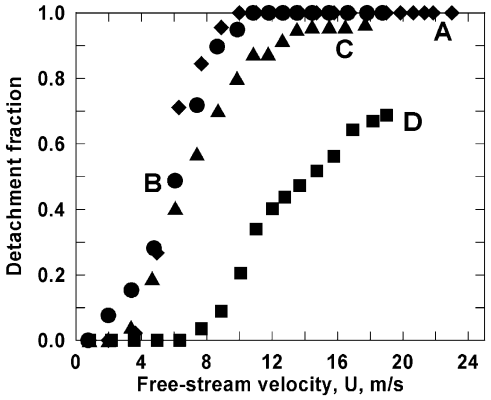

Fig. 8. Detachment fraction versus free stream velocity for SSPOLY. The free-stream velocity increased almost linearly with time up to ~23 m/s in 150 s. Cases A–C have initial depositions of larger and more uniformly distributed diameter microspheres than case D.

moment created by the microsphere's drag (Stokesian drag is proportional to the diameter) overcomes the pull-off moment at lower velocities for larger diameters.

The effect of diameter for another microsphere-substrate material combination (stainless steel on glass) is shown in Fig. 8. Four cases involving SSPOLY microspheres are presented. Examination of microvideographs of the initial deposition before each case revealed two situations: one comprised of larger and more uniformly distributed diameter microspheres (denoted by A, B and C), and the other by smaller and more broadly distributed diameter microspheres (denoted by D). The microspheres for case D have a relatively larger U_{th} than that of cases A–C (~14 m/s versus ~6 m/s). This, for the same reasons as before, is a consequence of smaller diameter.

Smaller microparticles of the same material require a larger flow velocity to achieve the same amount of detachment. In order to investigate the near ~100% detachment of smaller microparticles, the flow must be accelerated to a higher flow velocity. If flow acceleration is kept close to the previous case, then a longer period of flow acceleration is required. For the GL32, LY30, and SSPOLY microparticle cases, the flow was accelerated from 0 to 23 m/s over a 150 s period.

Experiments involving simultaneous changes in two or more variables require more interpretation. The composite effect of shape and material for microparticles of nominally the same diameter can be elucidated by comparing the results of experiments using the GL32 and LY30 microparticles. Fig. 9 compares the detachment fraction versus free-stream velocity of the two types. Lycopodium spores are nearly spherical with small protuberances on their surfaces. Consequently, they have less contact area with the substrate and reduced pull-off force and moment. In addition, they are subjected to more drag force and moment than a sphere of the same Stokes diameter. Therefore, they detach at a smaller free-stream velocity. This is observed in the figure, where the GL32 microspheres detach between ~4 and ~23 m/s, and the LY30 microparticles detach between ~9 and ~23 m/s. U_{th} for LY30 is almost 2.5 times greater than that for GL32 (~16 versus ~6 m/s). Differences between their surface adhesion energies also could play a role, but that for LY30 on glass is not known.

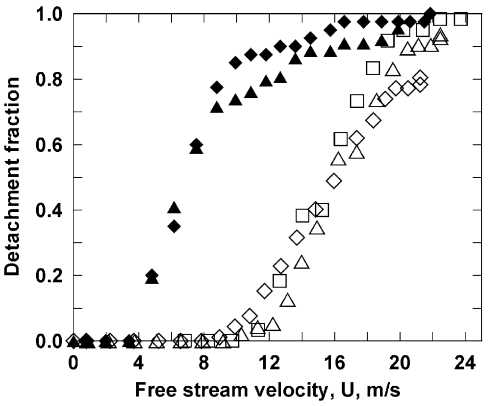

Fig. 9. Detachment fraction versus free-stream velocity: The solid symbols show two repeated experiments of LY30 microparticles and the open symbols show three repeated experiments of GL32 microspheres. The free-stream velocity increased almost linearly with time up to ~23 m/s in 150 s in both experiments.

All of these results can be supported further through modeling, which is presented in the following section.

4. Modeling results

Fig. 1 presents a schematic of a microparticle attached to a surface and the forces acting on it at the moment of detachment. Four forces are shown: the lift force, F_L, in the upward vertical direction, the gravitational force, F_g $(=mg)$, and the adhesion force, F_{po}, in the downward vertical direction and the drag force F_d, in the forward horizontal direction. Three detachment modes are possible:

- Direct lift-off, where

$$F_L > F_{po} + mg. \tag{3}$$

- Sliding, where

$$F_d > k_s(F_{po} + mg - F_L). \tag{4}$$

- Rolling, where

$$(1.4R)F_d + aF_L > a(F_{po} + mg). \tag{5}$$

Here k_s is the static coefficient of friction. The factor 1.4 in Eq. (5) accounts for the non-uniformity of the flow field (O'Neill, 1968).

The pull-off force, F_{po}, is the force required to pull the microparticle vertically from the surface. Johnson and Greenwood (1997) used the Leonard–Jones potential to calculate the pull-off force at the DMT-JKR transition (Derjaguin, Muller, & Toporov, 1975; Johnson, Kendall, & Roberts, 1971). According to these calculations, the smooth-surface pull-off force is 1.61R, 1.51R, and 1.52R for SS70, GL72 and GL32, respectively. The results of Cheng et al. (2002) show that the rough-surface

pull-off force is 1% of its smooth-surface value for the standard deviation of heights on the substrate used.

The contact radius at separation, a, is evaluated according to the JKR theory for a smooth surface

$$a = \left(\frac{6\pi\gamma R^2}{4K}\right)^{1/3}, \tag{6}$$

where γ is surface energy of adhesion. K is the composite Young's modulus given by

$$K = \frac{4}{3}\left[\frac{(1-\nu_1^2)}{E_1} + \frac{(1-\nu_2^2)}{E_2}\right]^{-1}. \tag{7}$$

E_1 and E_2 are the values of Young's modulus and ν_1 and ν_2 are the values of Poisson's ratio for the microsphere and the surface, respectively.

In the present work, the JKR theory and the results of Johnson and Greenwood (1997) are used even though the adhesion force distribution in the contact area may not be symmetric around the microparticle center. The lift force is obtained from Mollinger and Nieuwstadt (1996). They measured the mean lift force on 120 and 218 μm-diameter microspheres attached to a wall. For $0.3 < R^+ < 2$, they obtained

$$F_L^+ = (56.9 \pm 1.1)R^{+(1.87\pm0.04)}, \tag{8}$$

where $F_L^+ = F_L/\rho\nu^2$ and $R^+ = Ru^*/\nu$. The drag force is modeled as Stokesian (because the microparticles are embedded completely within the viscous sublayer) and modified for wall (O'Neill, 1968) and slip (Friedlander, 1977) effects

$$F_d = (3\pi\mu\, dV)f, \tag{9}$$

where V is the flow velocity and μ is the absolute viscosity of the air and the factor f ($f = 1.7009$) accounts for the wall effect.

Soltani and Ahmadi (1994) proposed a sublayer model for the turbulent burst-sweep event. According to this model

$$u^+ = 1.74y^+ + 0.1y^{+2} \tag{10}$$

and

$$w^+ = 0.54u^+, \tag{11}$$

where $u^+ = u/u^*$ and $y^+ = yu^*/\nu$. If there is no burst-sweep event, then $u^+ = y^+$. They performed a direct numerical simulation of microparticle entrainment in a turbulent channel flow. Their results show that during a turbulent burst-sweep event (Soltani & Ahmadi, 1995)

$$u^+ = \Phi y^+, \tag{12}$$

where the mean of Φ is 1.84 with minimum and maximum values of 1.6 and 2.14, respectively.

In the present experiments, the microparticles were embedded completely in the viscous sublayer. For this situation, supported by the results of Yung et al. (1989), the velocity in Eq. (9) was evaluated assuming that $u^+ = y^+$. However, some microparticles could detach by turbulent burst-sweep events. Eqs. (10) and (11) explain the detachment of microparticles at lower flow velocities. As shown in Fig. 10, a significant reduction in U_{th} for an individual microparticle occurs if the microparticle is

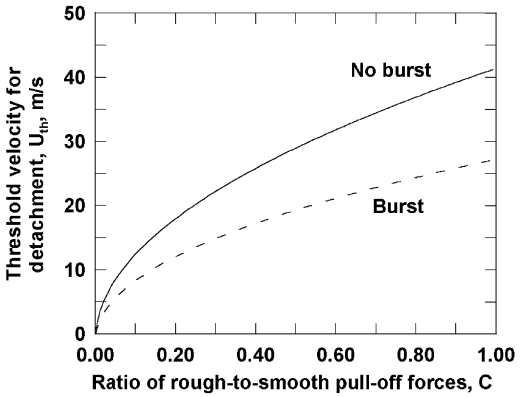

Fig. 10. Threshold velocity for detachment versus the reduction in pull-off force for SS70. Solid curve: computed with a model considering no turbulent burst. Dashed curve: computed with a model considering a turbulent burst.

Table 2
U_{th} (m/s) for various detachment modes of SS70, GL72, and GL32 microspheres

Detachment mode	SS70	GL72	GL32
Direct lift-off	58	77	133
Sliding	41	58	94
Rolling	3	7	14

detached by a turbulent burst-sweep event. This explains, in part, why there is a large range of flow velocities over which detachment occurs.

Table 2 presents the free-stream detachment velocities (in m/s) required assuming each possible mode of detachment for SS70, GL72, and GL32 microparticles. A coefficient of static friction of 0.6 is assumed. Image analysis on the frames at which detachment occurs show that detachment does not occur by direct lift-off, but rather through motion along the surface (rolling and/or sliding). The results shown in Table 2 suggest that rolling is the dominant mode for the present experiments. Detachment by sliding requires a much higher flow velocity (about 10 times greater). For sliding to occur, a static coefficient of friction of 0.03 or less would be required, which is not realistic.

Assuming that detachment occurs by rolling, further analysis can be done. In the following, the SS70 microsphere case is presented. The GL72 and GL32 cases show similar behavior.

The free-stream velocity required for rolling detachment with and without a turbulent burst-sweep event is shown in Fig. 10 for various reductions in the pull-off force. Such reductions would occur as a result of various surface roughnesses. It can be seen that a reduction in the pull-off force significantly lowers the flow velocity required for detachment. The results obtained from the present model are consistent with those of Soltani and Ahmadi (1994).

The measured values of U_{th} for the SS70, GL72 and GL32 cases are shown with the model results in Fig. 11. The experimental uncertainties, assessed at 95% confidence, also are shown.

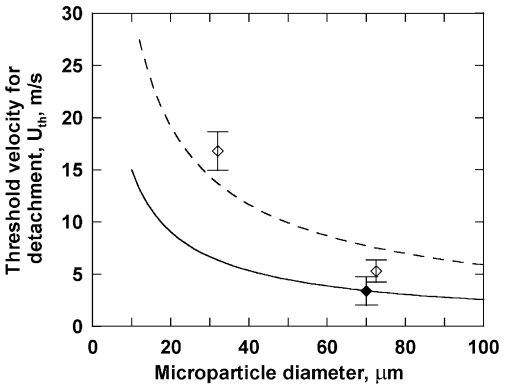

Fig. 11. Threshold velocity for detachment versus microparticle diameter for glass (dashed curve and open symbols) and stainless steel (solid curve and solid symbol) microparticles on glass. The symbols show the experimental measurements with their uncertainties.

These results assume rolling detachment with no turbulent burst-sweep events and a rough-surface pull-off force equal to 1.05% of its smooth-surface value. The results compare reasonably well with the measurements considering several limiting factors: (a) the model generates a single-detachment flow velocity while the experiments reveal a range of velocities, (b) the model uses the mean value of the microparticle diameter and macroscopic properties and (c) the model assumes no turbulent burst-sweep event even though some microparticles may detach with burst-sweep events of varying intensities.

Comparisons between the moments of the pull-off, drag, lift and gravity forces in the range of variables considered in the present work show that the lift and the gravity moments are orders of magnitude less than the drag and pull-off force moments. Consequently, for the range of values considered in the present experiments, U_{th} is determined by a balance between the pull-off force moment (which is independent on the flow velocity) and the drag force moment (which increases with the flow velocity).

5. Sensitivity analysis

The sensitivity of the threshold velocity for detachment, U_{th}, to various physical factors identified in the model were analyzed. Five factors were considered. These were the surface energy of adhesion (γ), the microparticle radius (R), the intensity of turbulent burst (Φ), the ratio of rough pull-off force to smooth pull-off force (C), and the Hertzian stiffness (K). The sensitivity was determined by examining the effects of the above factors on the response (U_{th}) using the design of experiments (DOE) method with a full factorial design layout (Davies, 1960). An illustration of the technique is shown in Brach, Li, and Dunn (2000).

U_{th} was determined analytically using a moment balance, as described in Eq. (5). The role of experiments in sensitivity analysis is to validate the analytical model with its factors used to estimate U_{th} and to set a range of nominal values for the factors. The response was calculated for combinations of the high and low values of the factors which are $\pm 10\%$ of the nominal values:

γ (0.15 J/m^2), R (35 μm), Φ (1), C (0.0105), K (8.41E10 N/m^2). Results indicate that the factors affect the response in the following order and directions: γ (60.1%), R (−53.9%), Φ(−42.9%), C(40.9%), K(−12.9%). Some second-order interactions also played a small role, mainly $R\gamma$(−5.8%), $\gamma\Phi$(−5.42%), and $C\gamma$(5.4%). Higher-order interactions are negligible. Negative signs indicate inverse relationships and positive signs a direct relationship. For example, an increase in the microparticle radius R causes a decrease in the U_{th} while an increase in the surface energy of adhesion γ causes an increase in the U_{th}.

6. Summary and conclusions

Quantitative experimental results and qualitative visual observations of the detachment of various microspheres and microparticles from glass substrates were presented. Surface-resident microparticles were exposed to a linearly accelerating flow for a period of time, then to a constant velocity thereafter. Experimental repeatability was assessed by performing experiments under the same conditions several times. Results showed that the uncertainty in the threshold velocity for detachment was approximately 10–20%. This relatively low level of uncertainty was obtained by controlling experimental conditions including the relative humidity, the initial number density, the storage duration, and the surface preparation and microparticle counting techniques.

Two mechanisms of detachment were observed from the microvideographic records. These were rolling detachment induced directly by the flow and detachment due to subsequent particle-to-particle collisions. Detachments due to collision were minimized by using sparse monolayers, were not counted and were not included in this study. Two phases of rolling detachment were identified, each depending on whether the level of the free-stream velocity was accelerating or constant. The transition from one to the other occurred when the flow velocity became constant. Rolling was determined to be the primary mechanism of detachment for sparse monolayers. Results of an AFM surface scan and the theory of Cheng et al. (2002) implied a large reduction in the pull-off force and low threshold velocities for detachment. This was substantiated by the experiments, which showed that the value of the threshold velocity for detachment was reduced significantly for a realistically rough surface. The value of the threshold velocity for detachment was determined by a balance between drag and pull-off moments. A sensitivity analysis was performed and the relative importance of five factors that affect the threshold velocity for detachment was established. Microparticle size and surface energy of adhesion were the two most significant factors.

Acknowledgements

Research described in this article was supported by Philip Morris Incorporated.

References

Bechert, D. W. (1996). Calibration of Preston tubes. *AIAA Journal*, *34*, 205–206.

Bowling, R. A. (1988). A theoretical review of particle adhesion. In K. L. Mittal (Ed.), *Particles on surfaces 1: Detection, adhesion and removal* (pp. 129–142). New York: Plenum Press.

Braaten, D. A., Paw, U. K. T., & Shaw, R. H. (1990). Particle resuspension in a turbulent boundary layer-observed and modeled. *Journal of Aerosol Science*, *21*, 613–628.

Brach, R. M., Li, X., & Dunn, P. F. (2000). Parameter sensitivity in microsphere impact and capture. *Aerosol Science and Technology*, *32*, 559–568.

Caylor, M. J. (1993). *The impact of electrically charged microspheres with planar surfaces under vacuum conditions*. Ph.D. Dissertation, University of Notre Dame.

Cheng, W., Brach, R. M., & Dunn, P. F. (2002). Surface roughness effects on microparticle adhesion. *Journal of Adhesion*, *78*, 929–965.

Corn, M. J. (1961). The adhesion of solid particles to solid surfaces II. *Journal of the Air Pollution Control Association*, *11*, 566–575.

Corn, M., & Stein, F. (1965). Re-entrainment of particles from a plane surface. *American Industrial Hygiene Association Journal*, *26*, 325–336.

Davies, O. L. (Ed.) (1960). *The design and analysis of industrial experiments.* New York: Imperial Hafner Publishing Company.

Derjaguin, B. V., Muller, V. M., & Toporov, Y. P. (1975). Effect of contact deformation on the adhesion of particles. *Journal of Colloid and Interface Science*, *53*, 314–326.

Fairchild, C. I., & Tillery, M. I. (1982). Wind tunnel measurements of the resuspension of ideal particles. *Atmospheric Environment*, *16*, 229–238.

Friedlander, S. K. (1977). *Smoke, dust and haze*. New York: Wiley.

Johnson, K. L., & Greenwood, J. A. (1997). An adhesion map for the contact of elastic spheres. *Journal of Colloid and Interface Science*, *192*, 326–333.

Johnson, K. L., Kendall, K., & Roberts, A. D. (1971). Surface energy and the contact of elastic solids. *Proceedings of the Royal Society of London, Series A*, *324*, 301–313.

Kim, H., Rockfold, L., & Russell, T. (1999). Adhesion to rough surfaces. In *American Physical Society Centennial Meeting Program*, Atlanta, GA.

Kline, S. J., Reynolds, W. C., Schraub, F. A., & Runstadler, P. W. (1967). The structure of turbulent boundary layers. *Journal of Fluid Mechanics*, *30*, 741–773.

Masironi, L. A., & Fish, B. R. (1964). Direct observation of particle reentrainment from surfaces. In B. R. Fish (Ed.), *Surface contamination* (pp. 55–59). Tennessee: Pergamon Press.

Mollinger, A. M., & Nieuwstadt, F. T. M. (1996). Measurements of the lift force on a particle fixed to the wall in the viscous sublayer of a fully developed turbulent boundary layer. *Journal of Fluid Mechanics*, *316*, 285–306.

Nicholson, K. W. (1988). A review of particle resuspension. *Atmospheric Environment*, *22*, 2639–2651.

O'Neill, M. E. (1968). A sphere in contact with a plane wall in a slow linear shear flow. *Chemical Engineering Science*, *23*, 1293–1298.

Phares, D. J., Smedley, G. T., & Flagan, R. C. (2000). Effect of particle size and material properties on aerodynamic resuspension from surfaces. *Journal of Aerosol Science*, *31*, 1335–1354.

Ranade, M. B. (1987). Adhesion and removal of fine particles on surfaces. *Aerosol Science and Technology*, *7*, 161–176.

Robinson, S. K. (1991). Coherent motions in The turbulent boundary layer. *Annual Review of Fluid Mechanics*, *23*, 601–639.

Schlichting, H. (1979). *Boundary layer theory* (7th ed.). New York: McGraw-Hill.

Sehmel, G. A. (1980). Particle resuspension: A review. *Environment International*, *4*, 107–127.

Smedley, G. T., Phares, D. J., & Flagan, R. C. (1999). Entrainment of fine particles from surfaces by gas jets impinging at normal incidence. *Experiments in Fluids*, *26*, 324–334.

Soltani, M. (1993). *Mechanisms of particle removal due to turbulent flow or substrate acceleration*. M.Sc. Thesis, Clarkson University.

Soltani, M., & Ahmadi, G. (1994). On particle adhesion and removal mechanisms in turbulent flows. *Journal of Adhesion Science and Technology*, *8*, 763–785.

Soltani, M., & Ahmadi, G. (1995). Direct numerical simulation of particle entrainment in turbulent channel flow. *Physics of Fluids*, *7*, 647–657.

Wu, Y., Cliff, I. D., & Russell, A. G. (1992). Controlled wind tunnel experiments for particle bounce-off and resuspension. *Aerosol Science and Technology*, *17*, 245–262.

Yung, B. P. K., Merry, H., & Bott, T. R. (1989). The role of turbulent bursts in particle re-entrainment in aqueous systems. *Chemical Engineering Science*, *44*, 873–882.

Zilliac, G. G. (1996). Further development of the fringe-imaging skin friction technique. *NASA Technical Memorandum 110425*.

Ziskind, G., Fichman, M., & Gutfinger, C. (1995). Resuspension of particulates from surfaces to turbulent flows: Review and analysis. *Journal of Aerosol Science*, *26*, 613–644.